

# Vertically Aligned Nanoplates of Atomically Precise Co<sub>6</sub>S<sub>8</sub> Cluster for Practical Arsenic Sensing

Anagha Jose<sup>a</sup>, Arijit Jana<sup>a</sup>, Tanvi Gupte<sup>a</sup>, Akhil S. Nair<sup>b</sup>, Keerthana Unni<sup>a</sup>, Ankit Nagar<sup>a</sup>, Amoghavarsha R. Kini<sup>a</sup>, B. K. Spoorthi<sup>a</sup>, Sourav Kanti Jana<sup>a</sup>, Biswarup Pathak<sup>b\*</sup>, Thalappil Pradeep<sup>a,c\*</sup>

<sup>a</sup>Department of Chemistry, DST Unit of Nanoscience (DST UNS) and Thematic Unit of Excellence (TUE), Indian Institute of Technology Madras, Chennai 600036, India. Email: [pradeep@iitm.ac.in](mailto:pradeep@iitm.ac.in)

<sup>b</sup>Department of Chemistry, Indian Institute of Technology Indore (IIT Indore), Indore 453552, India. Email: [biswarup@iiti.ac.in](mailto:biswarup@iiti.ac.in)

<sup>c</sup>International Centre for Clean Water, 2nd Floor, B-Block, IIT Madras Research Park, Kanagam Road, Taramani, Chennai 600113, India.

## Table of contents

Items	Description	Page no
1.	Experimental section	3
2.	Instrumentation	4
3.	Theoretical calculation	5
<b>Table S1</b>	Crystal data and structure refinement for the Co <sub>6</sub> nanocluster	8
<b>Table S2</b>	Atomic coordinates and equivalent isotropic displacement parameters for the Co <sub>6</sub> nanocluster	13
<b>Figure S1</b>	Time-dependent UV-vis absorption spectra of the Co <sub>6</sub> nanocluster indicating its stability	14
<b>Figure S2</b>	UV-vis absorption spectra of the Co <sub>6</sub> nanocluster in different solvents	15
<b>Figure S3</b>	Point EDS spectrum of the Co <sub>6</sub> nanocluster crystal	15
<b>Figure S4</b>	Atomic arrangements of the Co <sub>6</sub> nanocluster	16
<b>Figure S5</b>	Unit cell molecular packing of the Co <sub>6</sub> nanocluster along different axis	16
<b>Figure S6</b>	Different types of intercluster interactions	16
<b>Figure S7</b>	The full range ESI-MS spectrum of the Co <sub>6</sub> nanocluster	17

<b>Figure S8</b>	XPS spectra of the Co <sub>6</sub> nanocluster along with appropriate peak fitting	17
<b>Figure S9</b>	Comparison between experimental and simulated PXRD patterns	18
<b>Figure S10</b>	Thermogravimetric (TG) and differential thermogravimetric (DTG) analysis of the microcrystalline Co <sub>6</sub> nanocluster	18
<b>Figure S11</b>	Time-dependent density functional theory (TD-DFT) calculations	19
<b>Figure S12</b>	Electron density maps of Frontier molecular orbitals (FMOs) of the nanocluster	19
<b>Figure S13</b>	Optical microscopic images of ESD film	20
<b>Figure S14</b>	A large area FESEM	20
<b>Figure S15</b>	AFM micrographs of vertically aligned nanoplatelets	20
<b>Figure S16</b>	FESEM micrographs of three different films	21
<b>Figure S17</b>	UV-vis absorption spectra before and after electrospray deposition and ESI MS of the ESD film	21
<b>Figure S18</b>	FT-IR spectra of the Co <sub>6</sub> nanocluster in comparison with the ESD film	21
<b>Figure S19</b>	FESEM micrographs of the Co <sub>6</sub> sample drop casted on water	22
<b>Figure S20</b>	FESEM images of the Co <sub>6</sub> sample ESD on carbon cloth	22
<b>Figure S21</b>	FESEM images of the Co <sub>6</sub> electro sprayed sample on glycerol	22
<b>Figure S22</b>	FESEM images of the Co <sub>6</sub> electro sprayed sample on ethylene glycol	23
<b>Figure S23</b>	FESEM image of the EDS-Co <sub>6</sub> nanofilm modified glassy carbon electrode	23
<b>Figure S24</b>	Cyclic voltammograms of the ESD-Co <sub>6</sub> modified GC electrode in PBS	24
<b>Figure S25</b>	Cyclic voltammograms of bare GC electrode in PBS	24
<b>Figure S26</b>	Cyclic voltammograms of the Co <sub>6</sub> nanocluster-modified GC electrode in PBS	25
<b>Figure S27</b>	Relative energy profile of the interaction between As(OH) <sub>3</sub> and the Co <sub>6</sub> cluster	26
<b>Figure S28</b>	Charge density difference (CDD) analysis of As(OH) <sub>3</sub> binding to the Co <sub>6</sub> cluster	26

<b>Figure S29</b>	Interactions between As(OH) <sub>3</sub> and the Co <sub>6</sub> nanocluster and Badger charge analysis	27
<b>Figure S30</b>	Interfering ions study with different metal ions in PBS	27
<b>Figure S31</b>	Baseline corrected voltammetric profiles of recyclability of ESD-Co <sub>6</sub> modified GC electrode in PBS	28
<b>Figure S32</b>	UV-vis absorption spectra of ESD-film dissolved in DCM after 40 cycles of arsenic sensing experiments	28
<b>Figure S33</b>	Schematic diagram of the reaction vessel during the synthesis of the [Co <sub>6</sub> S <sub>8</sub> DPPE <sub>6</sub> Cl <sub>6</sub> ] nanocluster	30

## **1. Experimental section**

### **Chemicals used**

The borosilicate glass capillary was purchased from Sutter instruments, USA. All the materials were commercially available and were used without further purification. Cobaltous chloride ( $\text{CoCl}_2 \cdot 6\text{H}_2\text{O}$ , 97%) was purchased from Fisher Scientific. Sodium sulfide nonahydrate ( $\text{Na}_2\text{S} \cdot 9\text{H}_2\text{O}$ , 98%) was purchased from SRL. 1,2-bis(diphenylphosphino)ethane (97%) was purchased from Spectrochem. Sodium arsenite ( $\text{NaAsO}_2$ ) was purchased from S. D. Fine Chem. Ltd. HPLC grade dichloromethane (DCM), dimethylformamide (DMF), and methanol (MeOH) were purchased from Rankem.  $\text{CDCl}_3$  (99.99 % purity) was purchased from Sigma-Aldrich. All solvents and chemicals were used as such without further purification.

### **Synthesis of $\text{Co}_6$ cluster**

The  $\text{Co}_6$  cluster was synthesized at room temperature (25 °C) upon dissolving 0.016 g (0.124 mmol) of  $\text{CoCl}_2 \cdot 6\text{H}_2\text{O}$  in 2 mL of DMF. 0.2 g (0.5 mmol) of DPPE in 3 mL of DMF was added to the dissolved  $\text{CoCl}_2$  solution and stirred (1000 rpm) for 10 min. After that, 0.15 g  $\text{Na}_2\text{S} \cdot 9\text{H}_2\text{O}$  dissolved in 1 mL of methanol was added gradually to the stirred solution. In the course of the reaction, the bluish solution changes to dark brown with a greenish intermediate (shown in Figure S36). The final solution was kept for stirring for two days at room temperature. Purified cluster was dissolved in multiple solvents for further studies. The yield of the cluster is 85% in terms of cobalt precursors.

### **Electrospray deposition**

A home-built electrospray set-up was used for preparing the thin film. The electrospray source was made by pulling a borosilicate glass capillary of 1.5 mm outer diameter (OD) and 0.86 mm inner diameter (ID), using a micropipette puller instrument. It was cut into two pieces having an ID of 30-35  $\mu\text{m}$ . Freshly prepared  $\text{Co}_6$  cluster in DCM was filled inside the capillary using a micro-injector pipette tip. A spray plume was produced from the tip of the capillary by applying a DC potential of 2.75 to 3 kV between a platinum wire placed inside the capillary and the ground. The capillary tip was kept at a distance of 6 to 8 mm over the water substrate during the ESD process.

### **Preparation of working electrode**

The working electrode was made by carefully transferring the ESD-nanofilm onto a glassy carbon electrode. To reduce the structural damage of the nanoplates, we transferred it to a 3: 1 (v/v) nafion: DMF mixture and it was sonicated for 1 min to make a brownish dispersion. This dispersion was drop cast on a glassy carbon electrode and dried in vacuum for 1 h (the active

surface area was  $\approx 7 \text{ mm}^2$ ). Prior to each measurement, argon bubbling (exposure time = 10 min) was performed to remove dissolved oxygen. All the measurements were performed at room temperature ( $25 \text{ }^\circ\text{C}$ ).

## 2. Instrumentation

UV–vis absorption spectra of the cluster in their respective solution were recorded using a PerkinElmer Lambda 25 spectrophotometer in the wavelength range of 200–1100 nm. The slit width used for the measurement is 1 nm. Mass spectrometric measurements were performed using Waters Synapt G2-Si high-resolution mass spectrometer instrument equipped with time of flight (TOF) detector. Samples were measured using electrospray ionization (ESI) in the positive mode. An optimised instrumental condition (capillary voltage = 3 kV, source temperature =  $100 \text{ }^\circ\text{C}$ , desolvation temperature =  $150 \text{ }^\circ\text{C}$ , cone voltage = 0 V, source offset = 0 V, flow rate =  $20 \text{ }\mu\text{l}/\text{min}$ , desolvation gas flow =  $400 \text{ L}/\text{h}$ ) was used to record the spectrum. FT-IR spectra were measured using a JASCO-4100 spectrometer. A thin pallet of sample embedded with KBr was used for the measurement. X-ray photoelectron spectroscopy (XPS) measurements were done using an Omicron ESCA Probe spectrometer equipped with a polychromatic Al  $K\alpha$  X-ray source ( $h\nu = 1486.7 \text{ eV}$ ). The sample dissolved in DCM was drop-casted on an XPS sample stub and dried under ambient conditions. The pass energy for survey scans was kept at 50 eV and changed to 20 eV for specific regions for the measurements. Binding energies (BE) of the core levels were calibrated with C 1s BE set at 285 eV. Multinuclear NMR spectra were measured using a 500 MHz Bruker instrument (using  $\text{CDCl}_3$  solvents). TGA and DTG measurements were analyzed in the temperature range of 25 to  $700 \text{ }^\circ\text{C}$  using a NETZSCH STA 449 F3 Jupiter instrument. About  $\sim 5 \text{ mg}$  of crystalline sample was loaded in an alumina crucible for the measurement. Nitrogen was used as the environment with a flow rate of  $10 \text{ }^\circ\text{C}/\text{min}$ .

Optical microscopic images of the crystals and ESD film were observed using Leica Microscope. Surface morphology and elemental analysis were performed by FESEM–EDX (Thermo Scientific Verios G4 UC). Backscattered electrons and secondary electrons were used for imaging the surface at an accelerating voltage of 10 kV under high vacuum conditions. Surface morphology analysis of the ESD-film was performed by an Atomic Force Microscopy (AFM) system (Park Systems XE-100) in the non-contact mode.

## Single crystal XRD

Single-crystal X-ray diffraction data were recorded at 296 K using Bruker D8 VENTURE instrument. It equipped with a Mo K $\alpha$  X-ray source with the wavelength 0.71073 Å. A PHOTON 100 CMOS detector has been used to record the diffraction spots of multiple frames. A suitable crystal was mounted on a Kapton polymer loop with the help of paratone oil. The programme APEX3-SAINT (Bruker, 2016) was used for integrating the frames. A multi-scan absorption correction was done using the programme SADABS (Bruker, 2016). The structure was solved by SHELXT-2014 (Sheldrick, 2014) and refined by full-matrix least squares techniques using SHELXL-2018 (Sheldrick, 2018) computer programme. Hydrogen atoms were fixed at calculated positions and refined as riding model with C-H = 0.93 Å and Uiso(H) = 1.2 Ueq(C). Mercury 2020.2.0 software has been used for the visualization of the structure.

## Electrochemical sensing

All the electrochemical measurements were performed using a CH 600A (CH Instruments) electrochemical workstation. Arsenic sensing was carried out by cyclic voltammetry (CV) technique using NaAsO<sub>2</sub> dissolved in phosphate-buffered saline (PBS, pH ~ 7). The measurements were done with the following optimised parameters: scan rate of 50 mVs<sup>-1</sup>, sensitivity of 2 × 10<sup>-6</sup>, and potential range of -0.5 to 1 V. A conventional three-electrode cell was used with Ag/AgCl as the reference electrode and a Pt wire as a counter electrode. The working electrode was made by dispersing ESD nanofilm with 5.wt% Nafion binder. A few μL amount of this slurry was drop casted on a polished glassy carbon electrode (active surface area ≈ 7 mm<sup>2</sup>) for preparing the working electrode. Prior to each measurement, argon bubbling (exposure time = 10 min) was performed to remove the dissolved oxygen. All the measurements were performed at room temperature (25 °C).

## 3.Theoretical calculations

The periodic DFT calculations were done using Vienna Ab-Initio Simulation Package (VASP) by using Generalized gradient approximation of Perdew–Burke–Ernzerhof (PBE) functional.<sup>1,2</sup> Projector augmented wave (PAW) method is used for treating ion electron interactions.<sup>3</sup> The ionic relaxations have been carried out using a Conjugate gradient algorithm with convergence criteria of 10<sup>-4</sup> eV for minimum energy and 0.05 eV Å<sup>-1</sup> for Hellmann-Feynman forces on atoms. Due to the large size of the unit cells of the compounds, the Brillouin zone was sampled at the Gamma point (1×1×1). For the projected density of states (PDOS) calculation, a higher (2×2×2) K-mesh is used. The atomic charges are calculated using Bader charge analysis.<sup>4</sup> For

identifying the intercluster interactions, calculations of dimer and monomer clusters units are carried out with and without applying van der Waals correction using DFT-D3 method.<sup>5</sup>

The molecular DFT calculations were done using Gaussian 09 D.01 program.<sup>6</sup> B3LYP functional with Pople's 6-31G\* basis set was used for non-metal elements and LANL2DZ-ECP (effective core potential) was employed for Co atoms, respectively.<sup>7, 8</sup> The TD-DFT calculations considered 300 singlet-to-singlet excitation energies. Since a full ligand simulation with DPPE ligands is computationally expensive, we simplified the -Ph groups to -Me at the positions far from the Co<sub>6</sub> kernel while retaining the -Ph groups positioned close to the kernel. This allows us to reduce the computational cost without adapting a crude approximation of complete ligand simplification strategy. Kohn-Sham orbital analysis has been performed for identifying the orbital contribution in molecular orbitals and corresponding energies by using multi wave function 3.6 program.<sup>9</sup>

Table S1. Crystal data and structure refinement for Co<sub>6</sub> nanocluster.

Identification code	Co <sub>6</sub>	
Empirical formula	C156 H144 Cl6 Co6 P12 S8	
Formula weight	3213.10	
Temperature	296(2) K	
Wavelength	0.71073 Å	
Crystal system	Monoclinic	
Space group	P 21/c	
Unit cell dimensions	a = 20.4453(7) Å	α = 90°.
	b = 18.7380(6) Å	β = 102.515(2)°.
	c = 44.5513(15) Å	γ = 90°.
Volume	16662.2(10) Å <sup>3</sup>	
Z	4	
Density (calculated)	1.281 mg/m <sup>3</sup>	
Absorption coefficient	0.941 mm <sup>-1</sup>	
F(000)	6608	
Crystal size	0.200 x 0.150 x 0.130 mm <sup>3</sup>	
Theta range for data collection	2.401 to 20.000°.	
Index ranges	-19<=h<=19, -18<=k<=18, -42<=l<=42	
Reflections collected	165604	
Independent reflections	15508 [R(int) = 0.1709]	
Completeness to theta = 20.000°	99.8 %	
Absorption correction	Semi-empirical from equivalents	
Max. and min. transmission	0.7446 and 0.5706	
Refinement method	Full-matrix least-squares on F <sup>2</sup>	
Data / restraints / parameters	15508 / 1092 / 1693	
Goodness-of-fit on F <sup>2</sup>	1.077	
Final R indices [I>2σ(I)]	R1 = 0.0935, wR2 = 0.2479	
R indices (all data)	R1 = 0.1514, wR2 = 0.3071	
Extinction coefficient	n/a	
Largest diff. peak and hole	0.822 and -1.053 e.Å <sup>-3</sup>	

Table S2. Atomic coordinates ( $\times 10^4$ ) and equivalent isotropic displacement parameters ( $\text{\AA}^2 \times 10^3$ ) for  $\text{Co}_6$  nanocluster.  $U(\text{eq})$  is defined as one third of the trace of the orthogonalized  $U^{ij}$  tensor.

	x	y	z	$U(\text{eq})$
Co(1)	2822(1)	8672(1)	3246(1)	48(1)
Co(2)	2003(1)	8082(1)	3633(1)	52(1)
Co(3)	2986(1)	6995(1)	3822(1)	56(1)
Co(4)	3807(1)	7599(1)	3448(1)	51(1)
Co(5)	2440(1)	7217(1)	3186(1)	47(1)
Co(6)	3341(1)	8468(1)	3887(1)	57(1)
Cl(1)	2981(4)	9868(4)	1855(2)	163(3)
Cl(2)	-4(3)	6884(3)	1911(1)	113(2)
Cl(3)	3268(6)	11459(5)	4690(2)	226(4)
Cl(4)	157(4)	8589(7)	4683(2)	218(4)
Cl(5)	4045(6)	3651(5)	4192(2)	223(4)
Cl(6)	7085(9)	8165(10)	4104(5)	380(8)
C(1)	1581(7)	5707(7)	3001(3)	53(3)
C(2)	939(8)	5583(8)	3040(4)	72(5)
C(3)	784(8)	4940(10)	3159(5)	89(6)
C(4)	1244(9)	4408(9)	3223(4)	80(5)
C(5)	1869(9)	4508(8)	3193(4)	74(5)
C(6)	2051(8)	5168(8)	3076(4)	66(4)
C(7)	2160(7)	6178(7)	2540(3)	46(3)
C(8)	1778(8)	5798(10)	2307(4)	78(5)
C(9)	2021(10)	5486(10)	2083(4)	91(6)
C(10)	2680(11)	5580(10)	2074(5)	94(6)
C(11)	3094(10)	5973(9)	2290(5)	89(6)
C(12)	2818(8)	6267(9)	2522(4)	73(5)
C(13)	1030(6)	6926(7)	2646(3)	52(3)
C(14)	1093(7)	7519(8)	2422(3)	56(4)
C(15)	-246(8)	8089(8)	2358(4)	67(4)
C(16)	-53(9)	8639(9)	2564(4)	82(5)
C(17)	-525(11)	8971(10)	2696(5)	102(6)
C(18)	-1188(11)	8730(13)	2613(6)	118(8)
C(19)	-1396(10)	8193(12)	2407(6)	109(7)
C(20)	-911(9)	7859(10)	2281(4)	84(5)

C(21)	534(8)	8441(9)	1915(4)	71(4)
C(22)	914(9)	9025(9)	2064(5)	94(6)
C(23)	1072(10)	9566(12)	1874(6)	114(7)
C(24)	829(13)	9536(15)	1565(7)	132(9)
C(25)	446(13)	8977(14)	1418(6)	121(7)
C(26)	336(11)	8436(11)	1605(5)	102(6)
C(27)	3759(8)	8459(10)	2057(4)	71(4)
C(28)	3855(9)	7795(10)	2214(5)	84(5)
C(29)	4443(9)	7430(12)	2231(5)	100(6)
C(30)	4918(9)	7679(12)	2095(5)	98(6)
C(31)	4833(10)	8312(13)	1940(5)	112(7)
C(32)	4258(9)	8706(11)	1930(5)	101(6)
C(33)	2388(8)	8340(10)	1742(4)	69(4)
C(34)	2188(9)	7685(10)	1829(5)	92(5)
C(35)	1792(11)	7252(13)	1602(6)	121(7)
C(36)	1586(13)	7484(16)	1315(7)	139(10)
C(37)	1812(14)	8120(15)	1234(6)	133(9)
C(38)	2206(10)	8561(11)	1439(4)	92(5)
C(39)	2731(7)	8923(8)	2366(3)	62(3)
C(40)	3208(7)	9346(7)	2609(3)	56(3)
C(41)	3491(8)	10273(7)	3136(4)	64(4)
C(42)	4109(8)	10335(8)	3083(4)	71(5)
C(43)	4542(9)	10868(9)	3215(6)	101(7)
C(44)	4327(11)	11304(11)	3418(5)	110(7)
C(45)	3713(10)	11266(9)	3491(5)	93(6)
C(46)	3290(8)	10725(8)	3338(4)	77(5)
C(47)	2145(7)	10109(7)	2795(4)	56(4)
C(48)	1519(8)	9946(8)	2844(4)	72(5)
C(49)	986(9)	10345(9)	2726(5)	91(6)
C(50)	1071(9)	10949(9)	2568(5)	88(6)
C(51)	1693(10)	11130(10)	2510(5)	102(7)
C(52)	2220(9)	10711(9)	2621(4)	86(6)
C(53)	4687(9)	9435(11)	4197(4)	79(4)
C(54)	5205(10)	8995(12)	4342(6)	112(7)
C(55)	5844(12)	9102(16)	4318(7)	148(9)
C(56)	6000(11)	9676(17)	4150(6)	137(10)
C(57)	5467(11)	10108(14)	4006(5)	115(7)
C(58)	4828(9)	9995(11)	4026(4)	89(5)

C(59)	3952(9)	8995(11)	4632(4)	81(4)
C(60)	3828(12)	8334(13)	4733(5)	125(8)
C(61)	3955(14)	8160(16)	5040(6)	156(11)
C(62)	4180(14)	8694(19)	5248(6)	164(12)
C(63)	4301(13)	9360(16)	5159(5)	137(9)
C(64)	4147(13)	9499(14)	4853(5)	135(9)
C(65)	3439(9)	10107(9)	4203(4)	81(4)
C(66)	2781(9)	10163(10)	4305(5)	92(5)
C(67)	2412(11)	11551(10)	4036(6)	105(5)
C(68)	2058(11)	11265(10)	3762(6)	107(6)
C(69)	1877(10)	11679(13)	3502(7)	122(7)
C(70)	2061(10)	12389(12)	3508(6)	107(6)
C(71)	2425(12)	12695(14)	3764(7)	134(8)
C(72)	2588(11)	12277(11)	4023(6)	112(7)
C(73)	1796(14)	11056(14)	4479(6)	148(6)
C(74)	1244(13)	10704(16)	4308(7)	165(6)
C(75)	582(14)	10728(16)	4352(7)	181(7)
C(76)	545(16)	11122(18)	4611(7)	192(8)
C(77)	1067(14)	11492(17)	4800(7)	181(7)
C(78)	1680(14)	11479(15)	4720(6)	166(7)
C(79)	574(7)	9016(8)	3667(4)	66(4)
C(80)	787(9)	9566(9)	3522(5)	83(5)
C(81)	419(10)	10191(10)	3455(5)	108(7)
C(82)	-206(11)	10252(12)	3533(6)	120(8)
C(83)	-430(11)	9693(13)	3684(6)	124(8)
C(84)	-42(9)	9100(10)	3750(5)	94(6)
C(85)	434(7)	7550(8)	3563(4)	64(4)
C(86)	48(9)	7674(9)	3281(5)	84(5)
C(87)	-410(9)	7195(10)	3128(5)	90(6)
C(88)	-484(10)	6562(10)	3265(5)	99(6)
C(89)	-101(10)	6406(10)	3541(5)	106(7)
C(90)	341(9)	6893(10)	3686(5)	98(6)
C(91)	1039(8)	8039(8)	4155(4)	69(4)
C(92)	1360(9)	8641(11)	4381(4)	97(5)
C(93)	1521(14)	9300(15)	4978(6)	133(7)
C(94)	2192(13)	9388(14)	5012(5)	128(8)
C(95)	2492(15)	9957(17)	5206(6)	153(10)
C(96)	2152(18)	10330(19)	5384(8)	183(13)

C(97)	1497(18)	10220(20)	5368(8)	211(17)
C(98)	1153(15)	9701(18)	5152(6)	184(14)
C(99)	1442(14)	7805(16)	4912(6)	150(6)
C(100)	1095(15)	7395(15)	5094(6)	168(7)
C(101)	1417(16)	6799(16)	5265(7)	181(7)
C(102)	2058(16)	6549(18)	5256(7)	183(8)
C(103)	2397(16)	6971(15)	5086(7)	174(7)
C(104)	2096(14)	7567(15)	4918(6)	154(6)
C(105)	2120(9)	5811(9)	4141(4)	82(4)
C(106)	1711(9)	5313(10)	3963(5)	99(5)
C(107)	1088(10)	5125(11)	4007(5)	113(5)
C(108)	853(11)	5452(11)	4240(5)	120(6)
C(109)	1249(10)	5963(12)	4422(5)	116(5)
C(110)	1869(9)	6145(11)	4364(4)	99(5)
C(111)	3433(11)	5981(12)	4480(4)	102(6)
C(112)	3308(15)	5457(15)	4676(6)	157(10)
C(113)	3730(20)	5430(20)	4971(8)	198(16)
C(114)	4238(19)	5890(20)	5052(7)	191(15)
C(115)	4330(20)	6410(20)	4872(7)	230(20)
C(116)	3935(14)	6440(14)	4596(6)	155(11)
C(117)	3191(9)	5229(8)	3923(4)	82(5)
C(118)	3925(9)	5192(10)	3936(5)	97(5)
C(119)	3837(10)	4044(10)	3474(6)	101(5)
C(120)	3651(11)	3339(12)	3407(6)	115(6)
C(121)	3386(13)	3094(13)	3104(7)	127(8)
C(122)	3315(11)	3580(13)	2882(6)	116(7)
C(123)	3454(10)	4291(12)	2946(6)	113(6)
C(124)	3725(11)	4495(12)	3263(6)	107(6)
C(125)	5100(13)	4401(14)	3879(6)	141(5)
C(126)	5577(13)	3990(16)	4089(6)	173(7)
C(127)	6264(13)	3997(18)	4102(7)	185(7)
C(128)	6434(16)	4553(17)	3929(7)	186(8)
C(129)	6032(13)	4968(17)	3706(7)	172(7)
C(130)	5322(13)	4894(16)	3688(7)	159(6)
C(131)	4998(8)	6811(9)	3114(4)	69(4)
C(132)	4588(9)	6268(10)	3030(5)	89(6)
C(133)	4769(10)	5702(11)	2859(6)	118(8)
C(134)	5321(10)	5730(10)	2753(5)	92(6)

C(135)	5737(9)	6302(11)	2823(5)	99(6)
C(136)	5555(9)	6870(11)	2989(5)	98(6)
C(137)	5128(8)	8285(9)	3218(4)	70(4)
C(138)	4987(8)	8451(9)	2901(5)	79(5)
C(139)	5232(10)	9033(10)	2774(5)	103(6)
C(140)	5658(10)	9505(10)	2953(5)	87(6)
C(141)	5758(12)	9415(12)	3249(6)	116(7)
C(142)	5541(10)	8800(10)	3408(5)	94(6)
C(143)	5445(8)	7316(10)	3729(4)	86(5)
C(144)	6156(13)	7180(20)	3712(7)	218(9)
C(145)	6390(30)	6960(30)	4390(12)	272(8)
C(146)	6150(20)	6340(30)	4221(10)	278(9)
C(147)	5880(20)	6220(30)	4481(11)	286(9)
C(148)	5910(20)	6420(30)	4795(12)	294(10)
C(149)	6280(20)	7050(30)	4888(11)	283(10)
C(150)	6570(20)	7360(20)	4657(11)	274(9)
C(151)	7580(20)	6960(30)	3982(9)	329(9)
C(152)	7460(20)	6280(30)	3846(9)	336(11)
C(153)	8070(20)	5910(30)	3853(10)	337(11)
C(154)	8630(30)	6330(30)	4004(10)	347(12)
C(155)	8840(20)	7020(30)	4134(11)	333(11)
C(156)	8190(20)	7330(30)	4120(10)	329(11)
P(1)	1838(2)	6535(2)	2851(1)	47(1)
P(2)	335(2)	7703(2)	2150(1)	69(1)
P(3)	2971(2)	8917(3)	2005(1)	69(1)
P(4)	2900(2)	9558(2)	2953(1)	52(1)
P(5)	2581(4)	11069(3)	4386(2)	116(2)
P(6)	3827(2)	9219(3)	4228(1)	70(1)
P(7)	1089(3)	8568(4)	4740(2)	120(2)
P(8)	1049(2)	8192(2)	3751(1)	61(1)
P(9)	2948(2)	6049(2)	4088(1)	71(1)
P(10)	4216(3)	4295(3)	3872(2)	116(2)
P(11)	4810(2)	7506(2)	3372(1)	62(1)
P(12)	6750(5)	7273(9)	4076(3)	236(5)
S(1)	3181(2)	7805(2)	2980(1)	50(1)
S(2)	3858(2)	8771(2)	3519(1)	51(1)
S(3)	1796(2)	8199(2)	3119(1)	50(1)
S(4)	2491(2)	9149(2)	3647(1)	59(1)

S(5)	2631(2)	7852(2)	4098(1)	64(1)
S(6)	1944(2)	6912(2)	3557(1)	56(1)
S(7)	3999(2)	7496(2)	3961(1)	64(1)
S(8)	3301(2)	6533(2)	3415(1)	59(1)

---

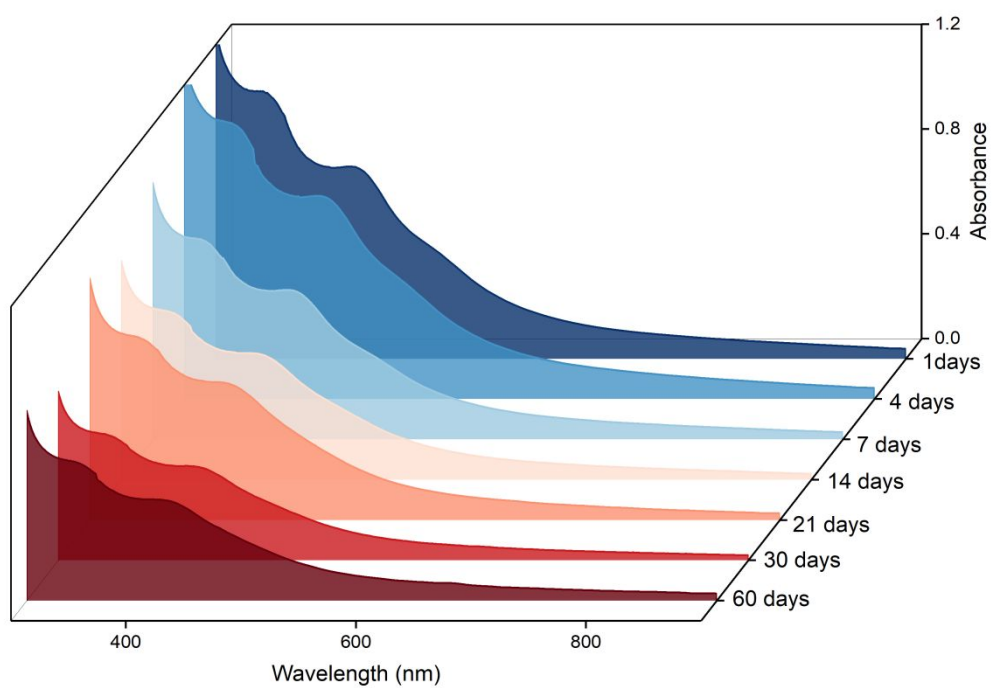


**Figure S1.** Time-dependent UV-vis absorption spectra of the Co<sub>6</sub> nanocluster in DCM, indicating its stability up to 60 days in ambient conditions.

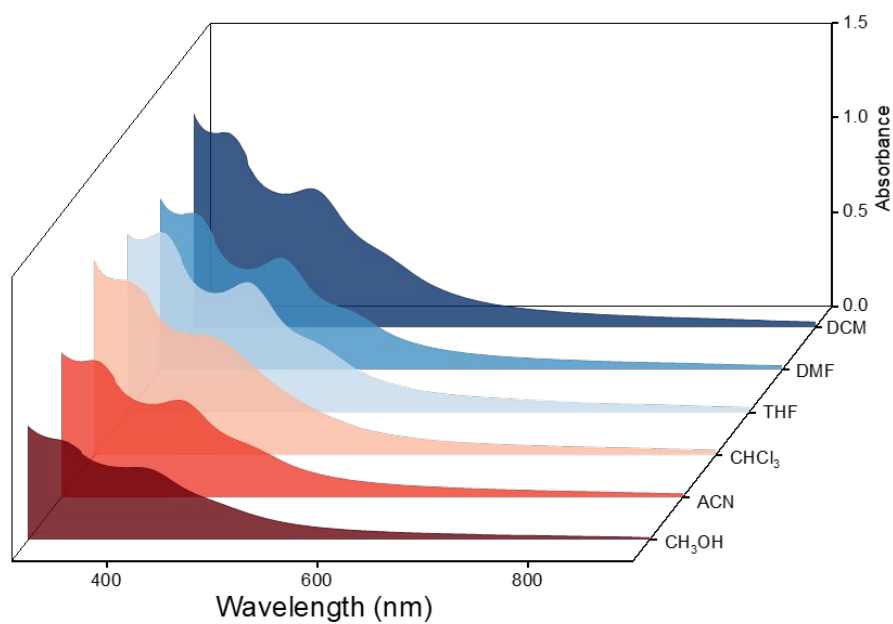


**Figure S2.** UV-vis absorption spectra of the  $\text{Co}_6$  nanocluster measured in different solvents. Identical peak patterns and positions were observed in all the solvents.

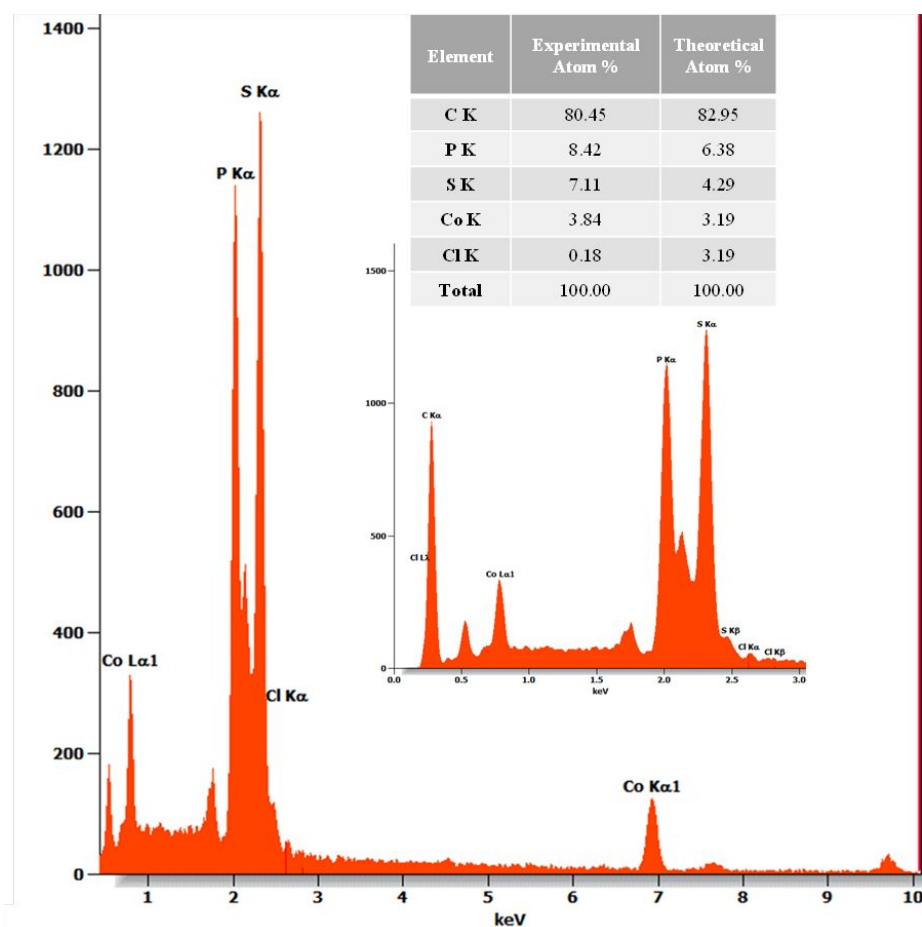


**Figure S3.** Point EDS spectrum of the  $\text{Co}_6$  nanocrystal. Inset shows the elemental composition.

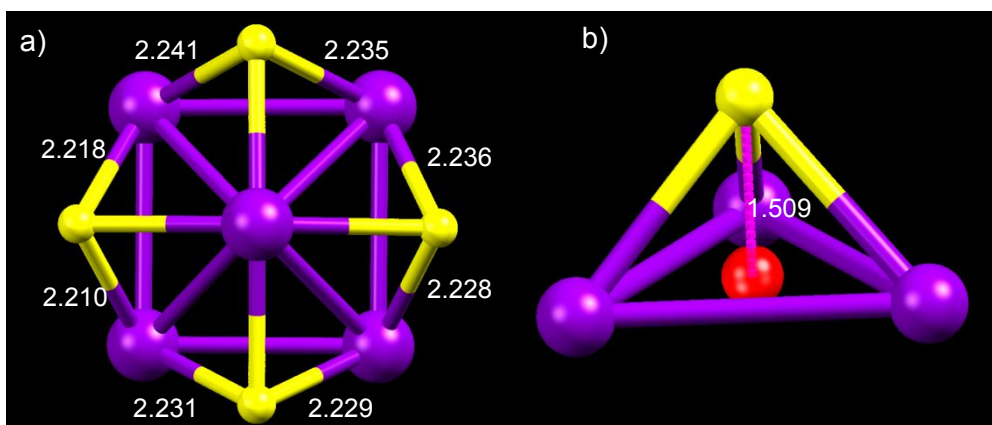


**Figure S4.** a) Front view of the  $\text{Co}_5\text{S}_4$  unit with marked Co-S bonds. b) The distance between the centroid of triangular facet to sulphur.

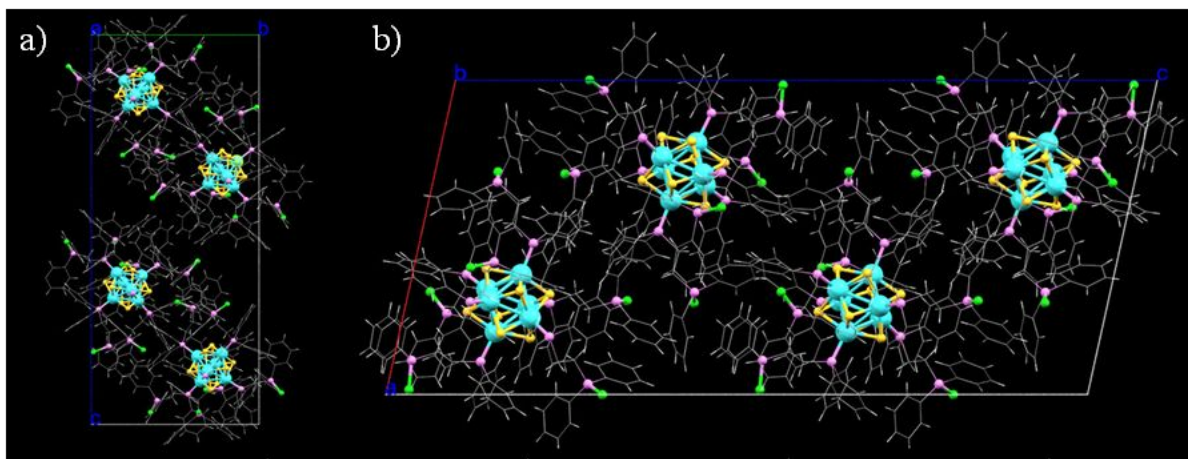


**Figure S5.** Unit cell molecular packing of the  $\text{Co}_6$  nanocluster along a) a, and b) b axis.

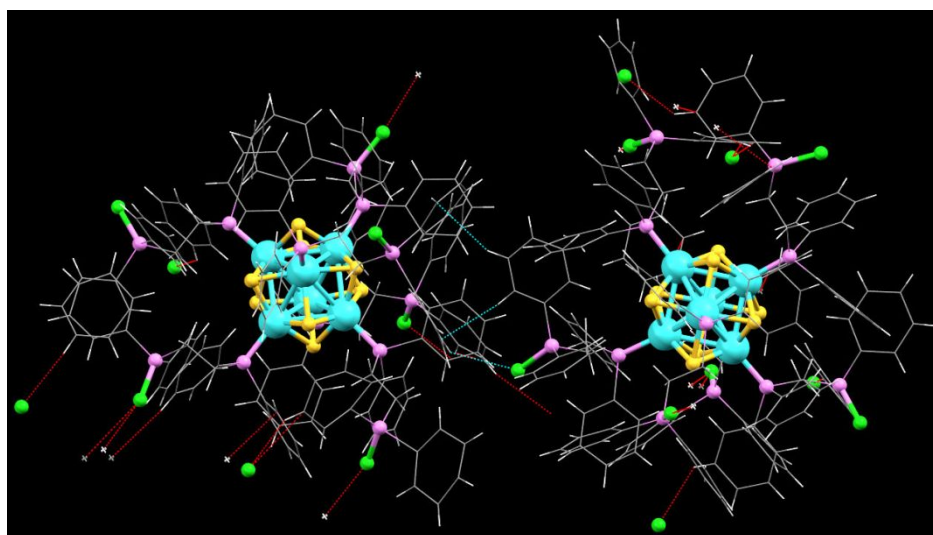


**Figure S6.** Different types of intercluster interactions responsible for intermolecular packing inside the crystal.

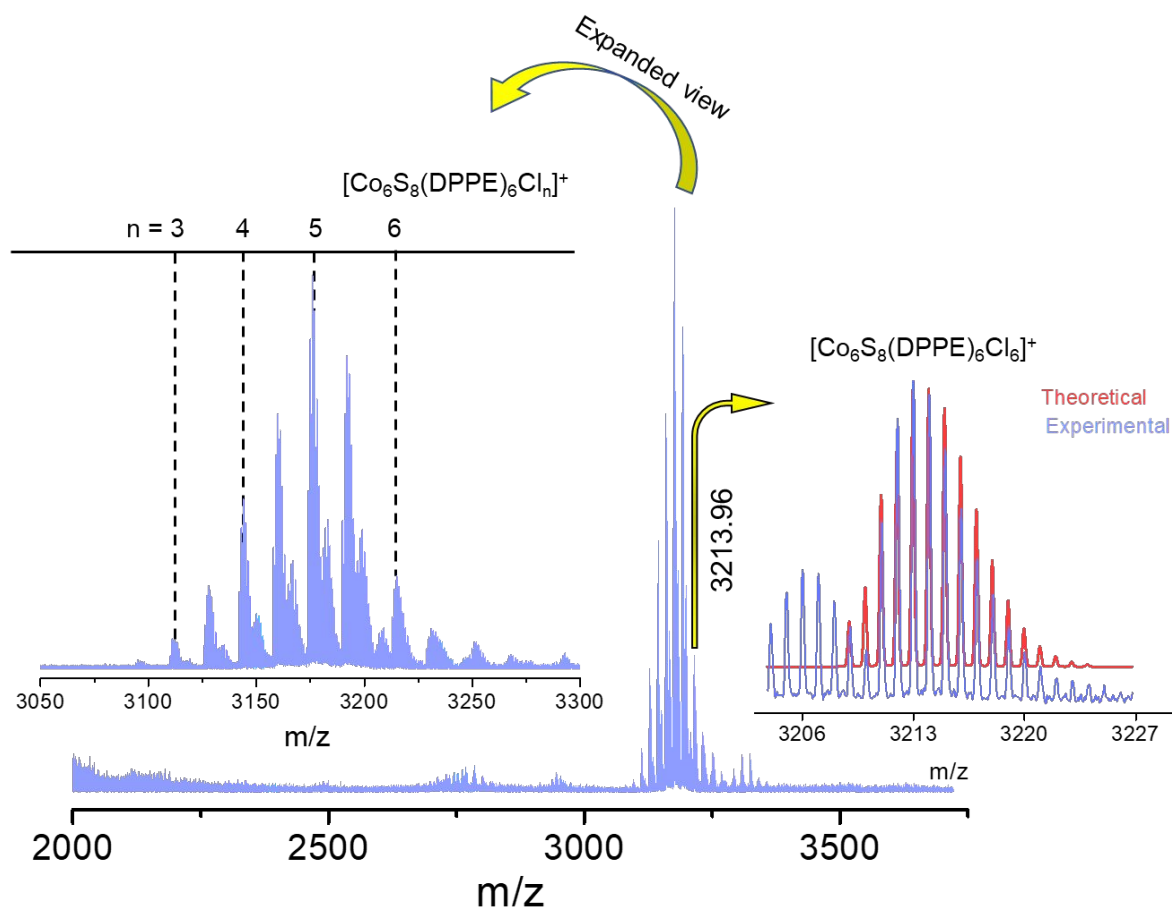


**Figure S7.** a) The full range ESI-MS spectrum in positive ion mode. The inset shows the exact matching of the isotopic distribution of the experimental with theoretical data.

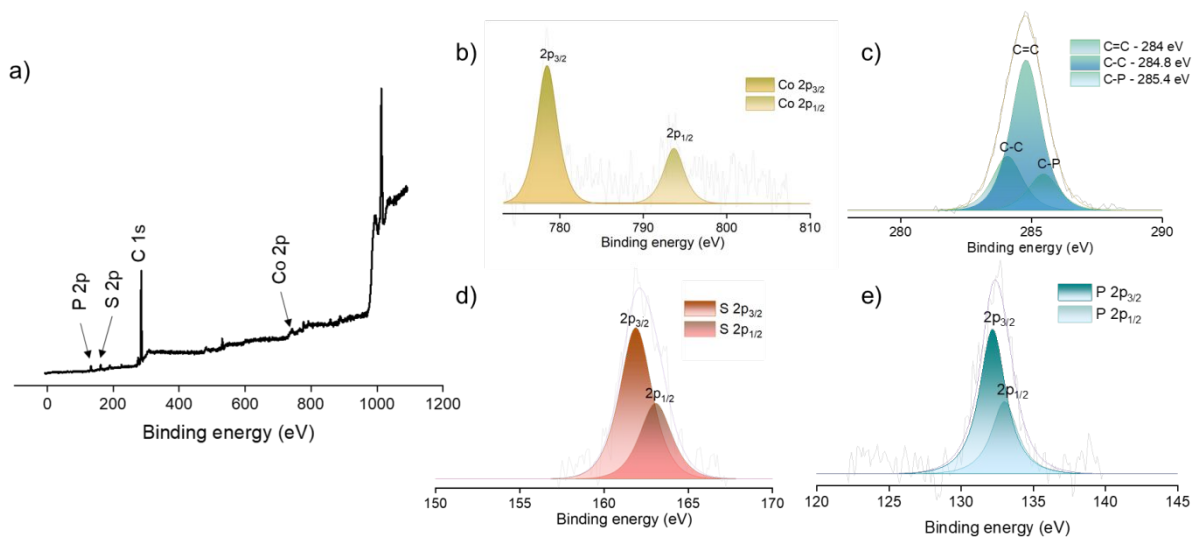


**Figure S8.** a) XPS survey spectrum of the  $\text{Co}_6$  nanocluster showed the spectral signature of respective elements. Spectral fitting of b) Co 2p, c) C 1s, d) S 2p and e) P 2p regions.

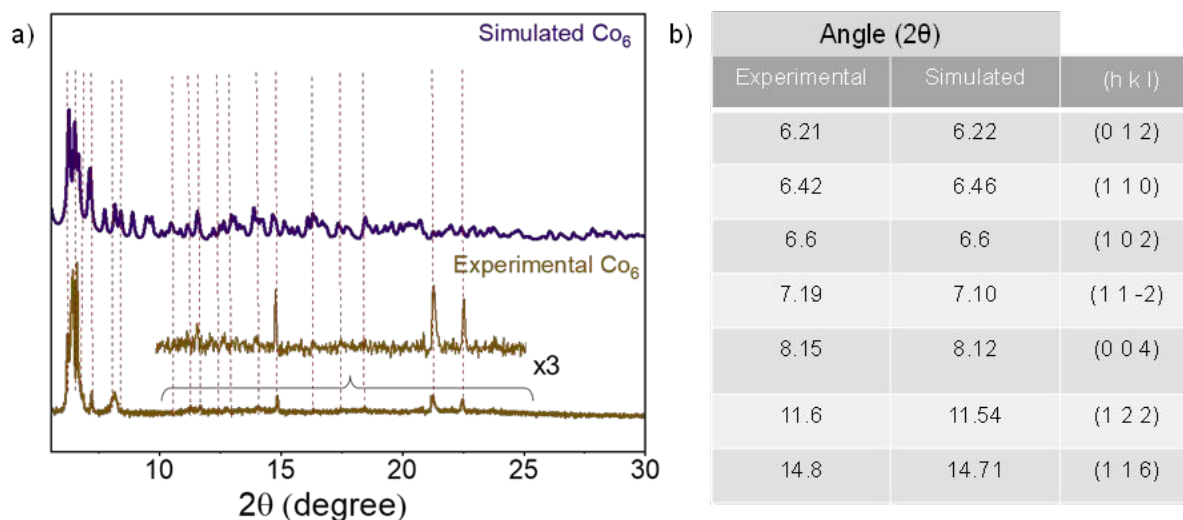


**Figure S9.** a) Comparison between the experimental and simulated PXRD patterns obtained from single crystals. Experimental spectrum in the  $10^\circ - 25^\circ$   $2\theta$  range is also expanded to see the features clearly. b) Analysis of the corresponding lattice planes.

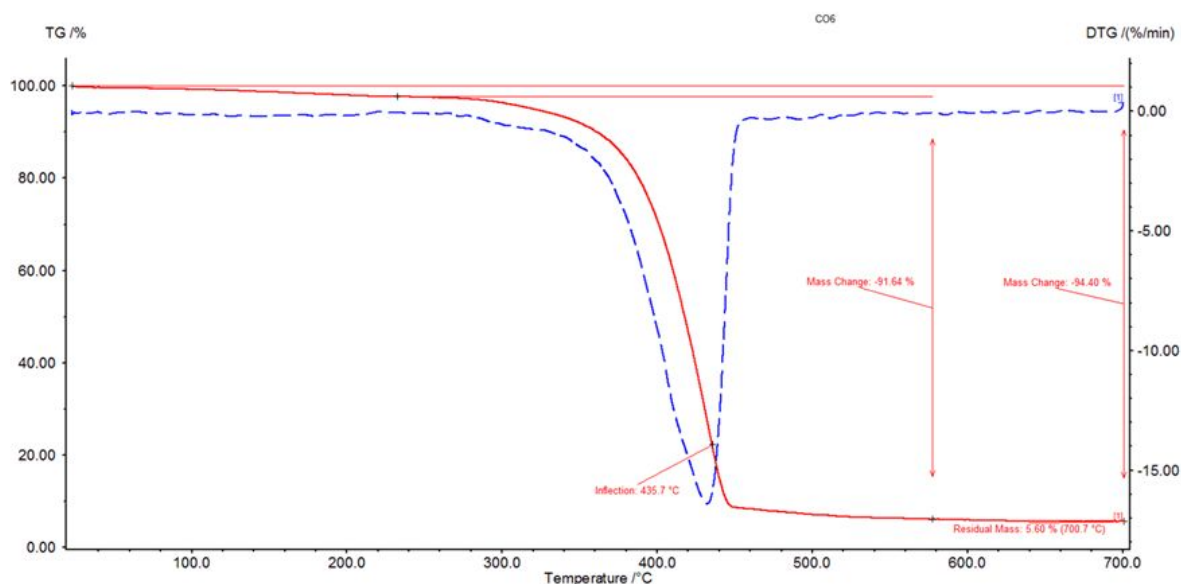


**Figure S10.** Thermogravimetric (TG) and differential thermogravimetric (DTG) analysis of the microcrystalline  $\text{Co}_6$  nanocluster in the heating range of  $25 - 700^\circ\text{C}$ . Solid line (red) indicate the TG and dotted line (blue) indicate the DTG profiles.

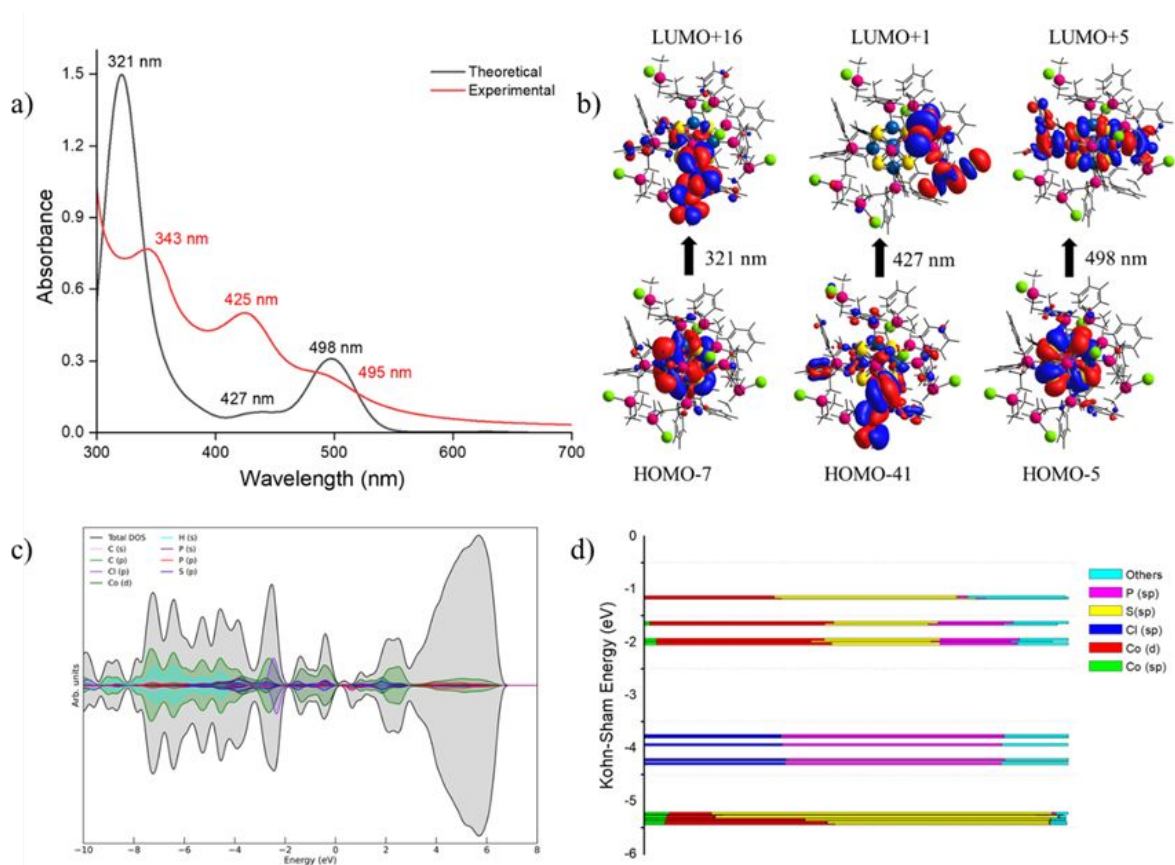


**Figure S11.** a) Comparison between the experimental and theoretical absorbance spectra of the Co<sub>6</sub> nanocluster. b) Electron density maps of the respective transitions at 321, 427, and 498 nm. c). Projected density of states (PDOS) analysis d). Kohn-Sham orbital contribution analysis.

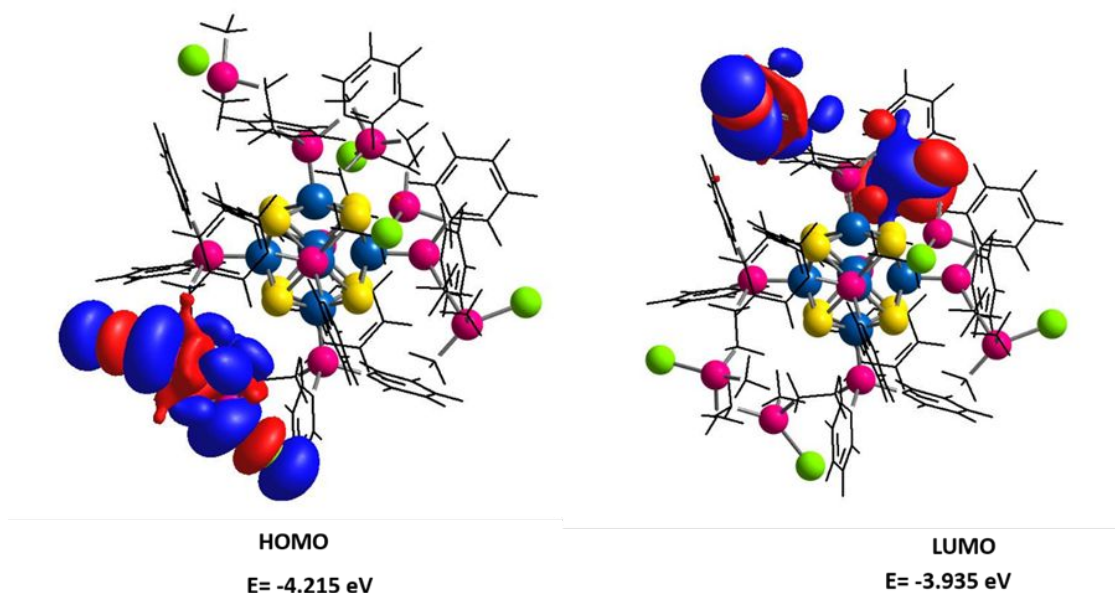


**Figure S12.** Electron density maps of Frontier molecular orbitals (FMOs) of the Co<sub>6</sub> nanocluster.

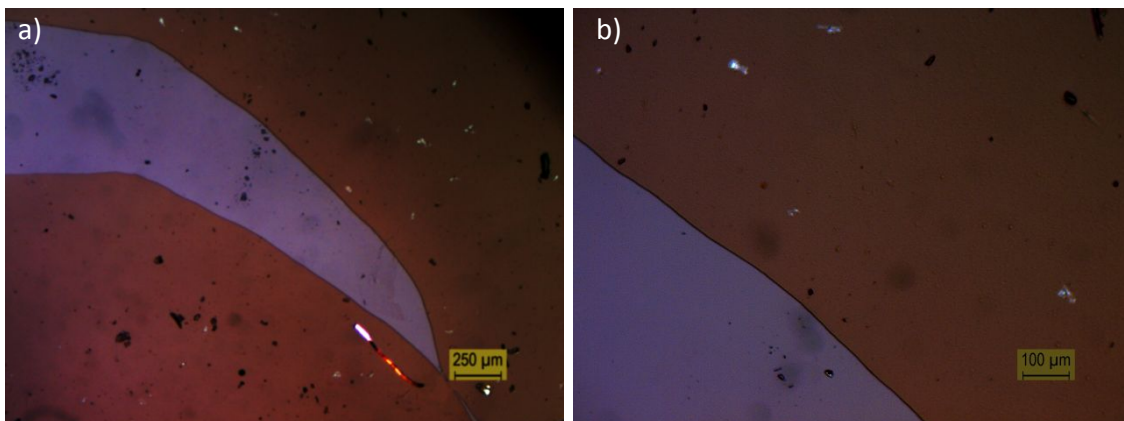


**Figure S13.** Optical microscopic images of the ESD film at different magnifications.

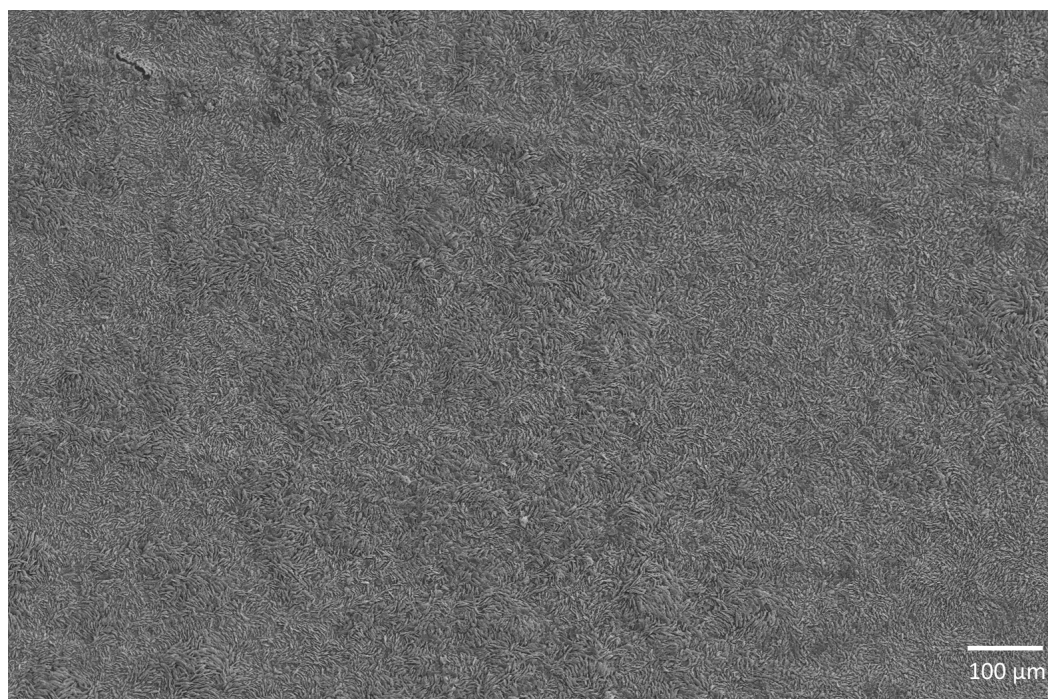


**Figure S14.** A large area FESEM micrograph demonstrated the uniform nature of the vertically aligned nanoplates.

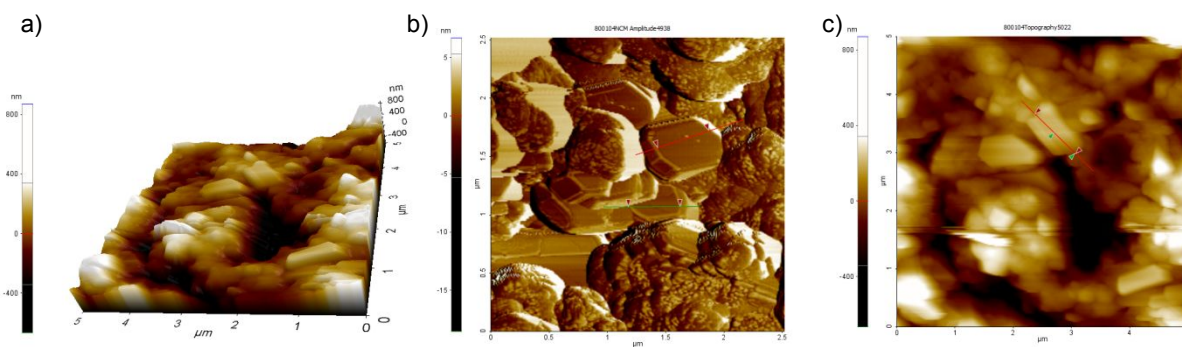


**Figure S15.** a) Large area, and b, c) magnified AFM micrographs of the vertically aligned nanoplates.



**Figure S16.** FESEM micrographs of three different films demonstrating reproducible nature of such nanostructures.

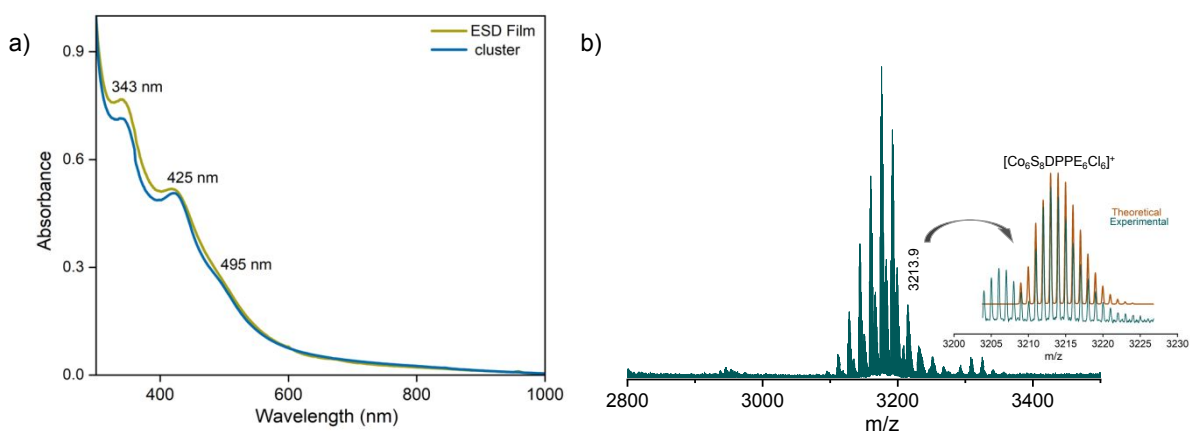


**Figure S17.** a) UV-vis absorption spectra before and after electro spray deposition. ESD film was dissolved in DCM for the measurement. b) ESI-MS spectrum in positive ion mode of the ESD film. Inset shows the exact matching of the isotopic distribution of the experimental and theoretical data.

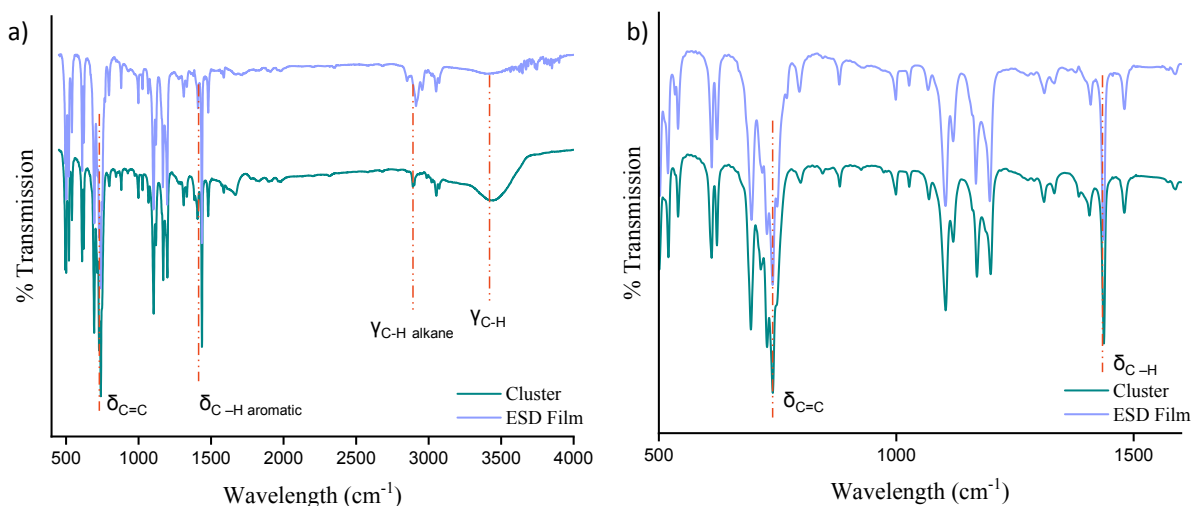


**Figure S18.** a) The full range FT-IR spectra of the  $\text{Co}_6$  nanocluster in comparison with ESD film. b) Expanded view of two different spectral regions indicate nearly identical vibrational spectral features.

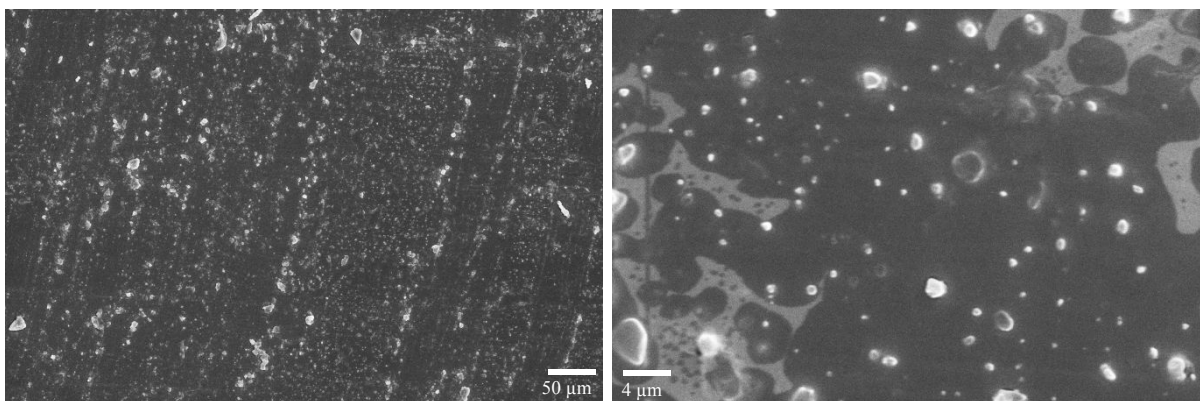


**Figure S19.** FESEM micrographs of the  $\text{Co}_6$  sample drop casted on water at different magnifications. No specific nanostructure was observed upon such drop casting.

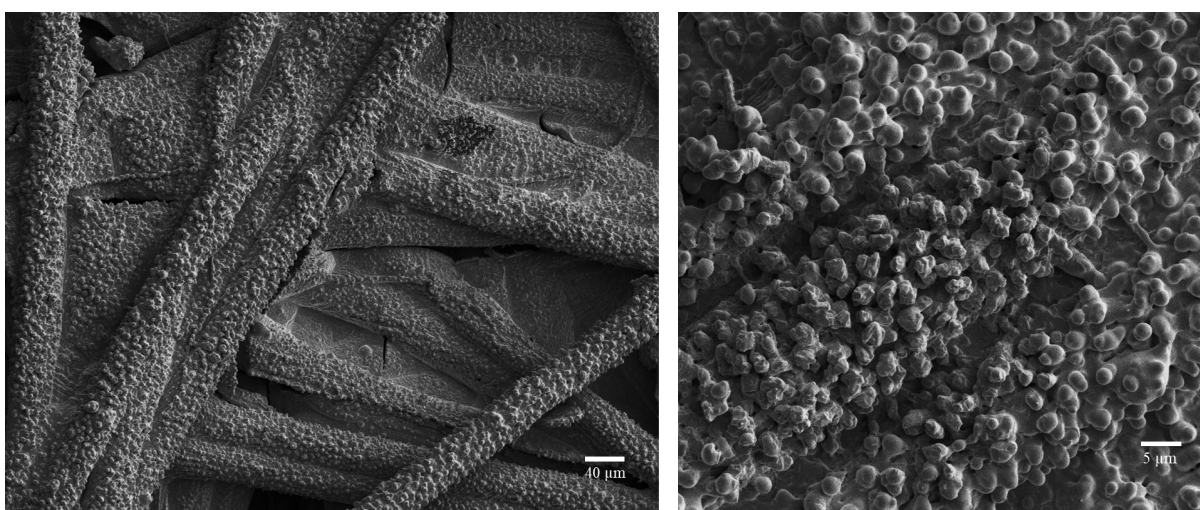


**Figure S20.** FESEM images of the carbon cloth at different magnifications after electro spray deposition of the  $\text{Co}_6$  nanocluster. No specific aligned nanostructure was observed.

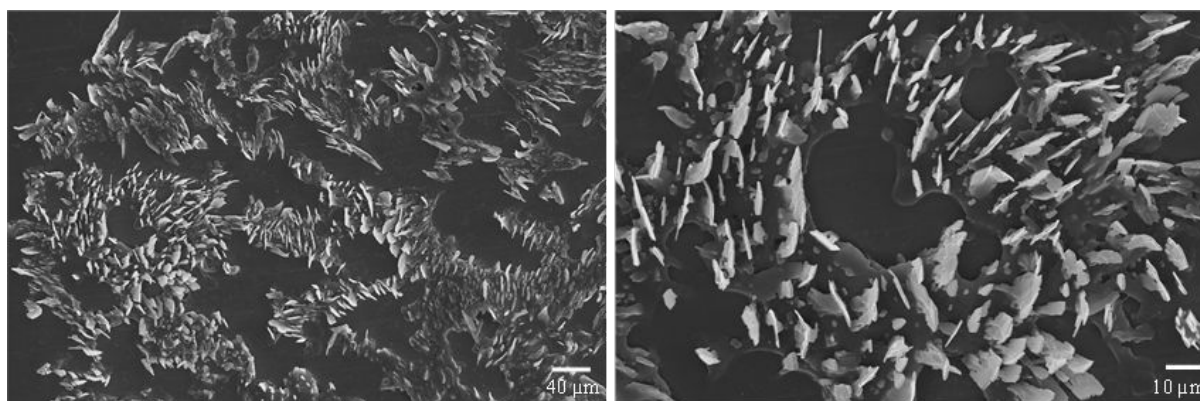


**Figure S21.** FESEM images of the  $\text{Co}_6$  electro sprayed sample on glycerol.

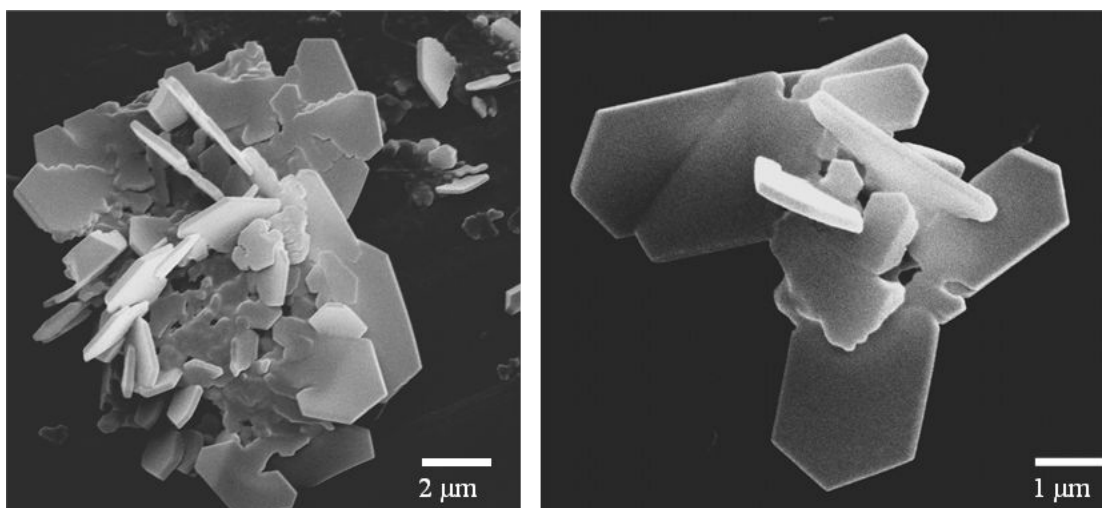


**Figure S22.** FESEM images of the Co<sub>6</sub> electrospayed sample on ethylene glycol.



**Figure S23.** FESEM image of ESD-Co<sub>6</sub> film modified glassy carbon electrode.

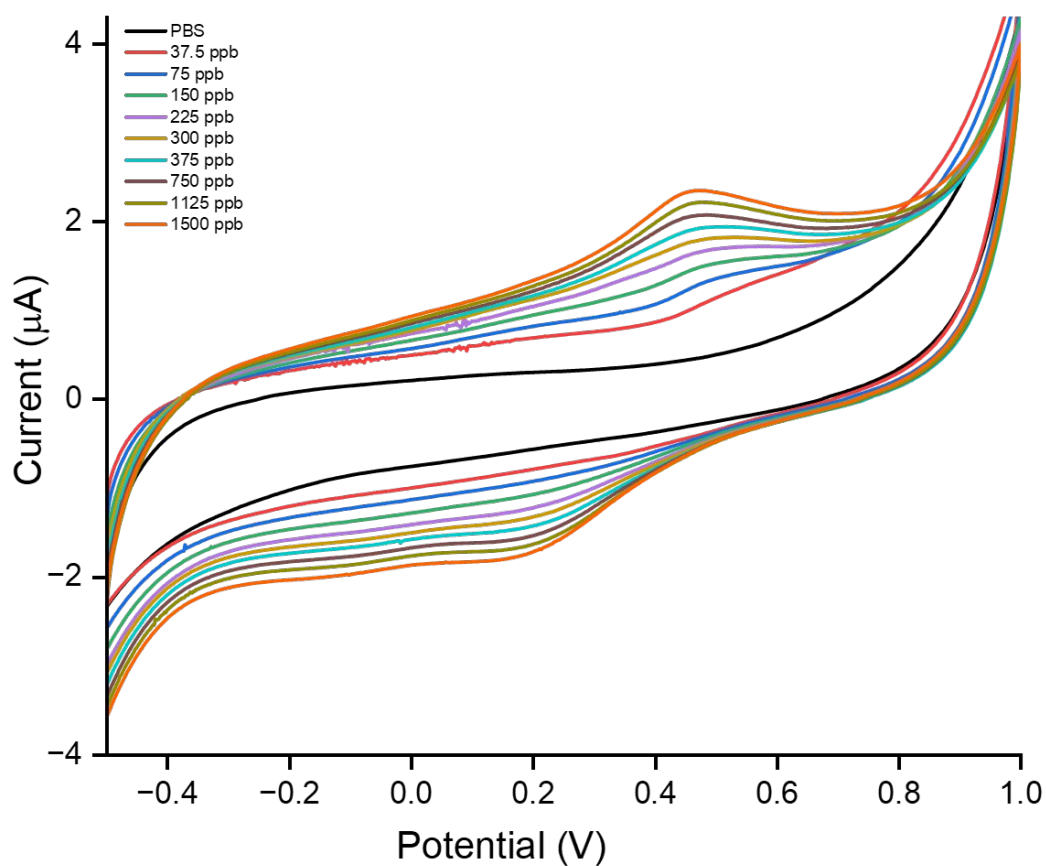


**Figure S24.** Cyclic voltammograms of ESD- $\text{Co}_6$  modified GC electrode in a buffer solution of pH 7 at a scan rate of  $50 \text{ mVs}^{-1}$  for various concentrations (37.5–1500 ppb) of  $\text{As}^{3+}$ .

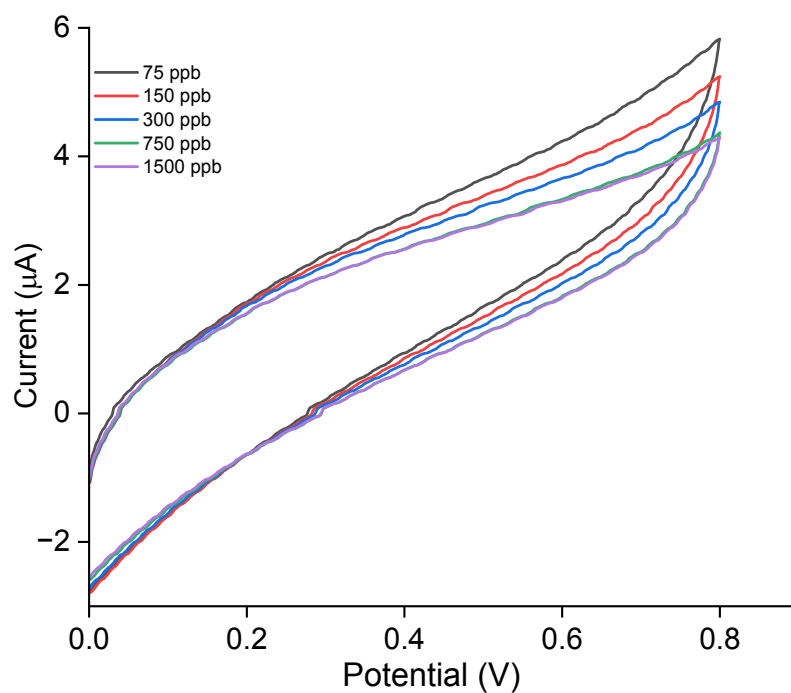


**Figure S25.** Cyclic voltammograms of bare GC electrode in a buffer solution of pH 7 at a scan rate of  $50 \text{ mVs}^{-1}$  for various concentrations (75–1500 ppb) of  $\text{As}^{3+}$ .

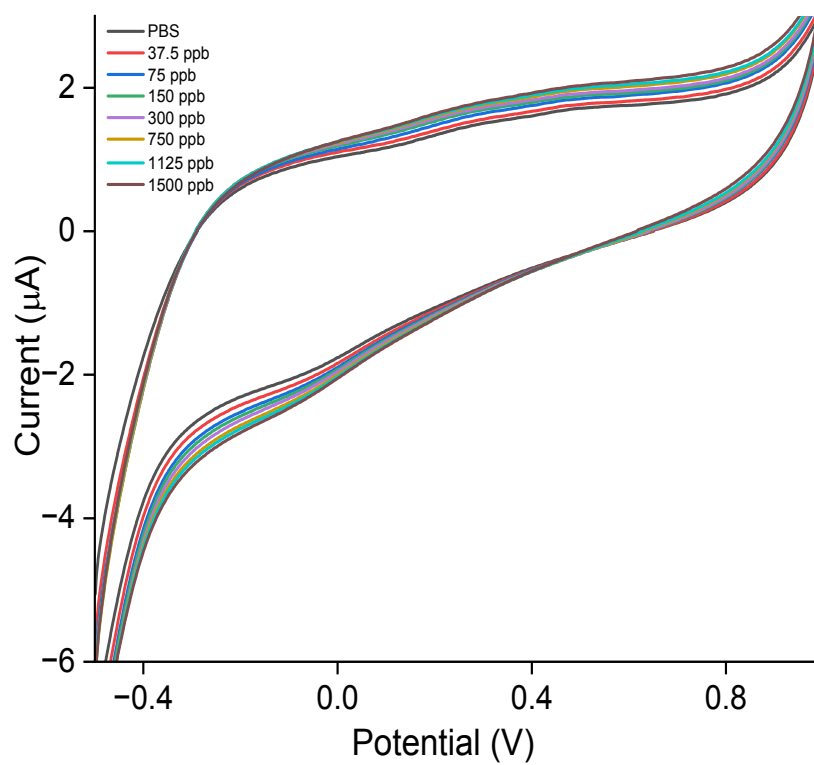


**Figure S26.** Cyclic voltammograms of Co<sub>6</sub> nanocluster modified GC electrode in a buffer solution of pH 7 at a scan rate of 50 mVs<sup>-1</sup> for various concentrations (37.5–1500 ppb) of As<sup>3+</sup>.

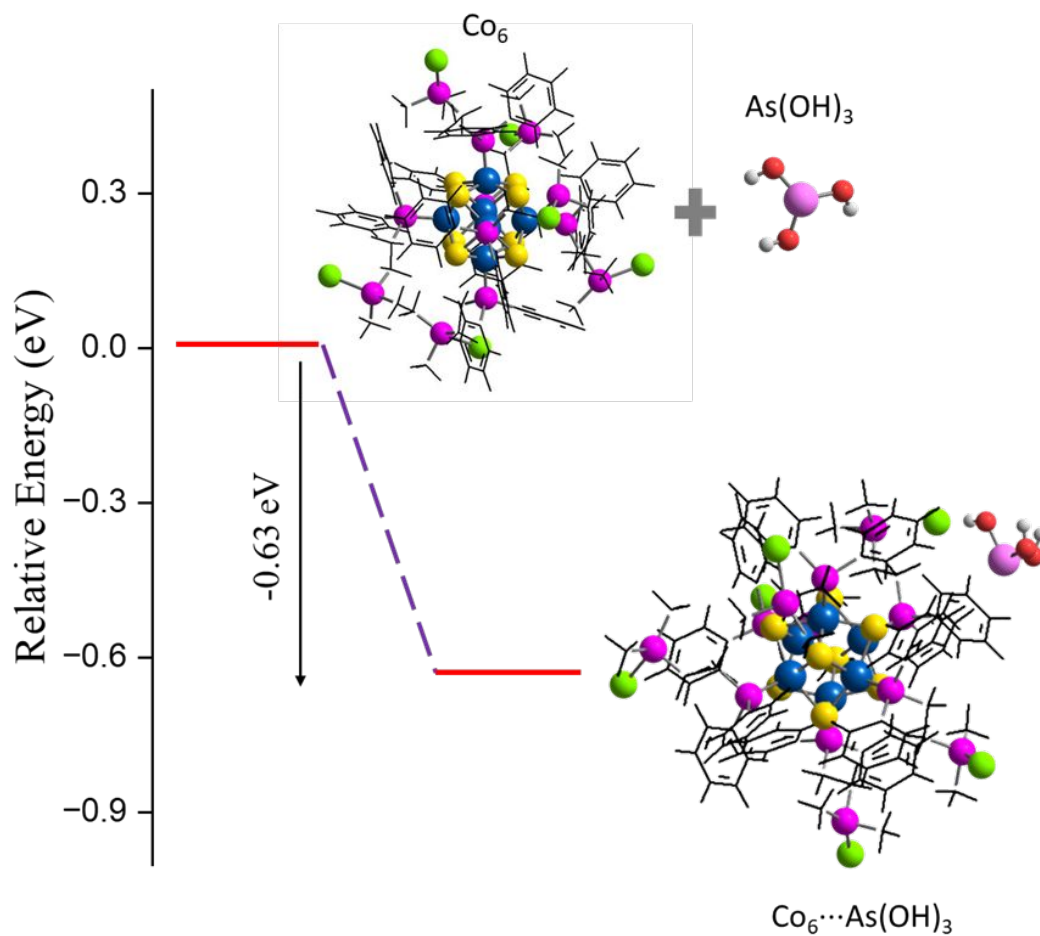


**Figure S27.** Relative energy profile of the interaction between  $\text{As}(\text{OH})_3$  and the  $\text{Co}_6$  nanocluster.

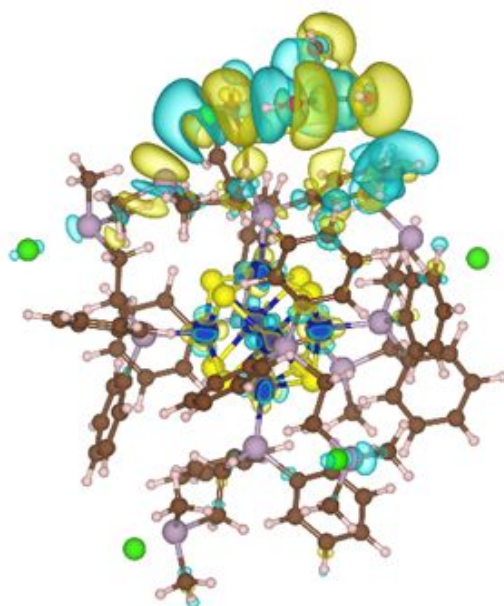


**Figure S28.** Charge density difference (CDD) analysis of  $\text{As}(\text{OH})_3$  binding to the  $\text{Co}_6$  cluster. The color code is, blue: Co, yellow: S, green: Cl, lavender: P, brown: C, pink: H. The positive and negative isosurfaces constructed at  $0.001 \text{ eV}/\text{\AA}^3$  are represented by cyan and yellow isosurfaces.

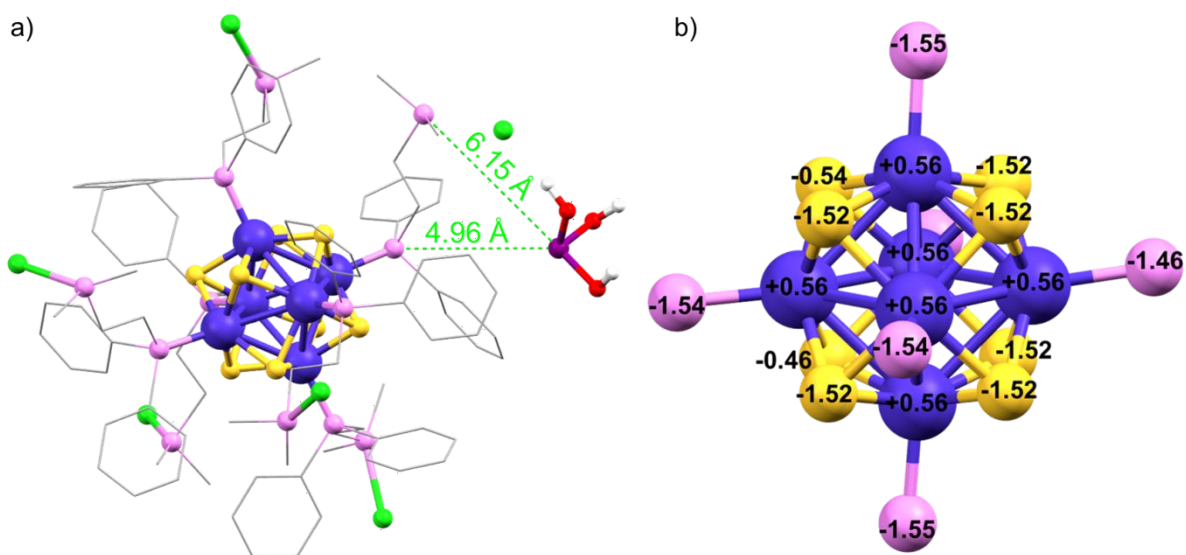


**Figure S29.** a) Interactions between As(OH)<sub>3</sub> and the Co<sub>6</sub> nanocluster. B) Bader charge analysis of the Co<sub>6</sub>S<sub>8</sub>P<sub>6</sub> unit.

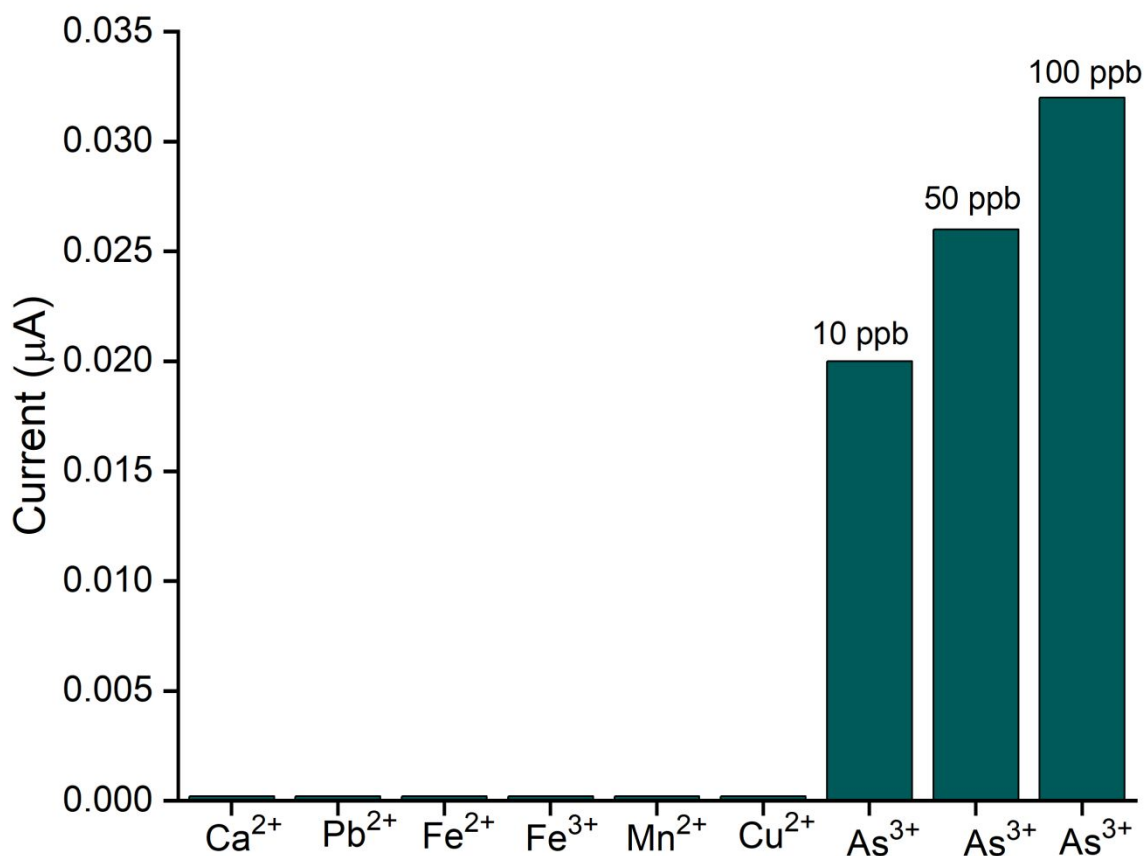


**Figure S30.** Interfering ions study with different metal ions (100 ppb Ca<sup>2+</sup>, Fe<sup>2+</sup>, Fe<sup>3+</sup>, Pb<sup>2+</sup>, Mn<sup>2+</sup>, and Cu<sup>2+</sup> added sequentially) and the response of arsenic in presence of all the metal ions in PBS.

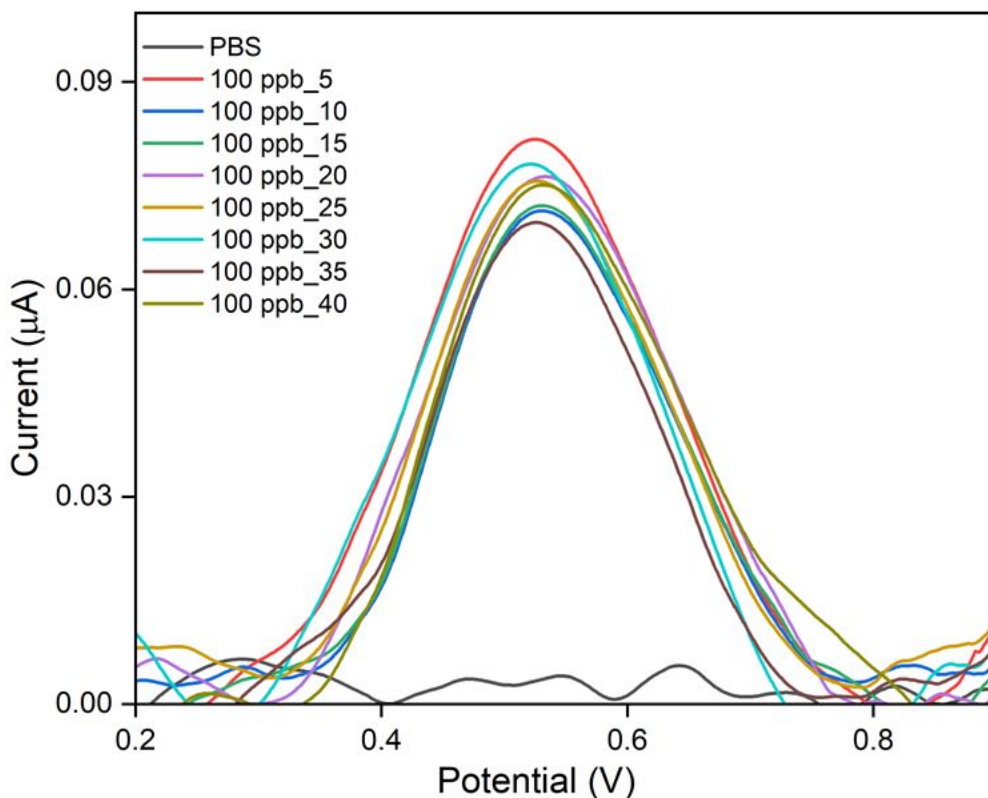


**Figure S31.** Baseline corrected voltammetric profiles of recyclability of ESD-Co<sub>6</sub> modified GC electrode in phosphate buffer solution of pH 7 up to 40 cycles at a scan rate of 50 mVs<sup>-1</sup> for a fixed concentration (100 ppb) of As<sup>3+</sup>.

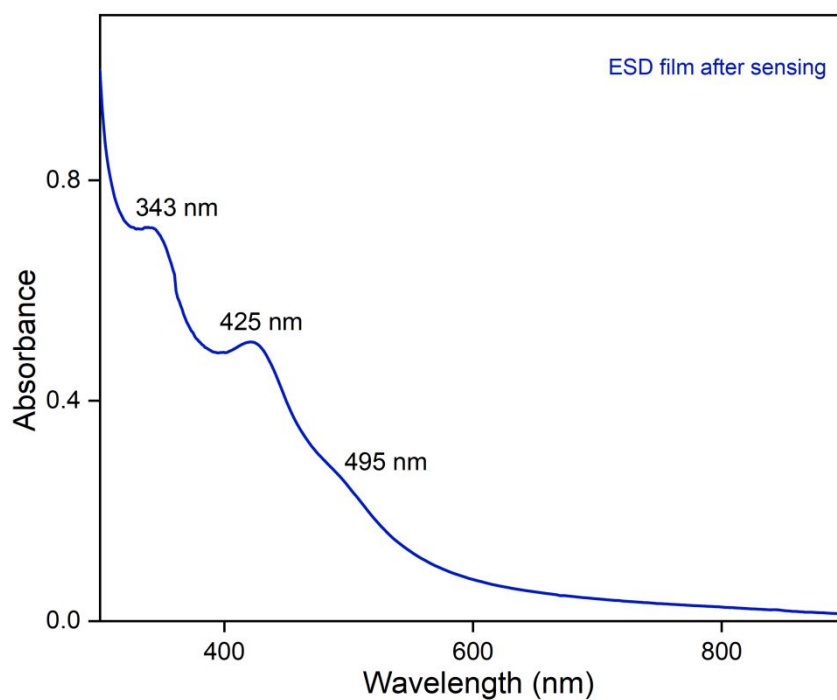


**Figure S32.** UV-vis absorption spectra of the ESD-film dissolved in DCM after 40 cycles of arsenic sensing experiments. The appearance of identical absorption bands indicating the essential structural integrity of the cluster after sensing.

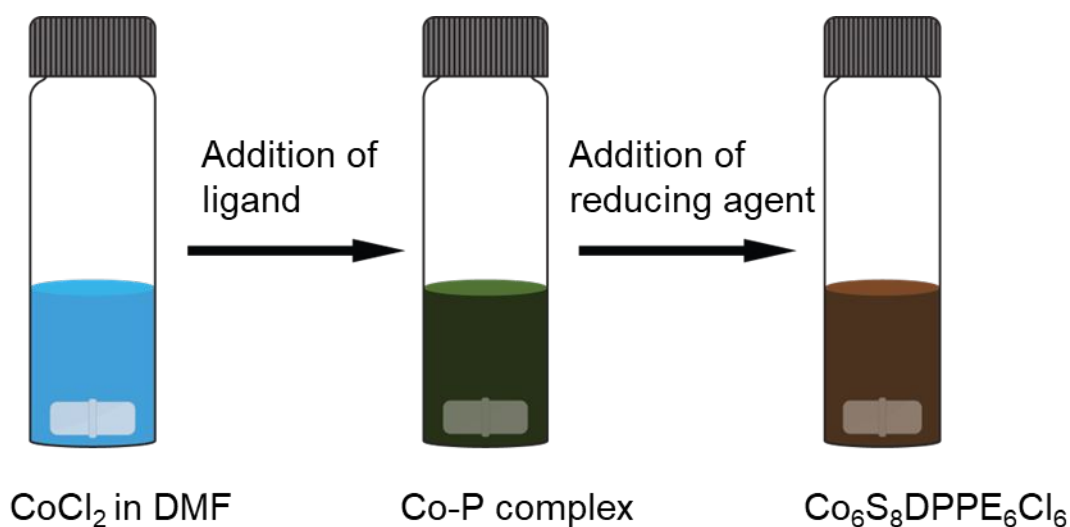


**Figure S33.** Schematic diagram of the reaction vessel during the synthesis of the  $[\text{Co}_6\text{S}_8\text{DPPE}_6\text{Cl}_6]$  nanocluster.

### Calculation of LOD

The theoretical limit of detection (LOD) was calculated using the following formula:<sup>10</sup>

$$\text{LOD} = \frac{3 \times \sigma}{M}$$

Where  $\sigma$  is the standard deviation of the blank sample and  $M$  is the slope of the linear fit.

Therefore,

$$\text{LOD} = \frac{3 \times 3.9225 \times 10^{-10}}{1.77 \times 10^{-7}} = 0.66 \text{ ppb}$$

### References

1. Kresse, G.; Hafner, J. Ab Initio Molecular-Dynamics Simulation of the Liquid-Metal–Amorphous-Semiconductor Transition in Germanium. *Phys. Rev. B: Condens. Matter Mater. Phys.* **1994**, *49*, 14251.
2. G. Kresse and J. Hafner, *Phys. Rev. B*, **1994**, *49*, 14251–14269.
3. Perdew, J. P.; Chevary, J. A.; Vosko, S. H.; Jackson, K. A.; Pederson, M. R.; Singh, D. J.; Fiolhais, C. Atoms, molecules, solids, and surfaces: Applications of the generalized gradient approximation for exchange and correlation. *Phys. Rev. B: Condens. Matter Mater. Phys.* **1992**, *46*, 6671.
4. Tang, W., Sanville, E., Henkelman, G. A grid-based Bader analysis algorithm without lattice bias, *J. Phys.: Compute Mater.* **2009**, *21* 084204.
5. S. Grimme, *J. Comput. Chem.*, **2006**, *27*, 1787–1799.

6. Frisch, M. J.; Trucks, G. W.; Schlegel, H. B.; Scuseria, G. E.; Robb, M. A.; Cheeseman, J. R.; Scalmani, G.; Barone, V.; Mennucci, B.; Petersson, G. A.; Nakatsuji, H.; et al. Gaussian 09, Revision D.01; *Gaussian, Inc.: Wallingford, CT*, **2009**.
7. Becke, A. D. Density-Functional Thermochemistry. III. The Role of Exact Exchange. *J. Chem. Phys.* **1993**, *98*, 5648-5652.
8. McLean, A. D.; Chandler, G. S. Contracted Gaussian Basis Sets for Molecular Calculations. I. Second Row Atoms, Z=11-18. *J. Chem. Phys.* **1980**, *72*, 5639–5648.
9. Lu, T.; Chen, F. Multiwfn: A Multifunctional Wavefunction Analyzer. *J. Comput. Chem.* **2012**, *33*, 580-592.
10. Miller, J. N. Basic Statistical Methods for Analytical Chemistry. Part 2. Calibration and Regression Methods. A Review. *Analyst* **1991**, *116* (1), 3.